ELEVEN-VERTEX POLYHEDRAL DICARBAPLATINABORANE CHEMISTRY.* ASPECTS OF THE CHEMISTRY OF SOME *closo*-STRUCTURED {1,2,3-PtC_2B_8} SPECIES AND SOME RELATED COMPOUNDS

John D. KENNEDY[a], Bohumil ŠTÍBR[b,**], Tomáš JELÍNEK[b], Xavier L. R. FONTAINE[a] and Mark THORNTON-PETT[a]

[a] *School of Chemistry, University of Leeds, Leeds LS2 9JT, England*

[b] *Institute of Inorganic Chemistry, Academy of Sciences of the Czech Republic, 25068 Řež near Prague, The Czech Republic*

Received June 18, 1992
Accepted April 7, 1993

The reaction of the ten-vertex *nido* anions $[6,9\text{-}C_2B_8H_{10}]^{2-}$, $[6\text{-Me-}6,9\text{-}C_2B_8H_9]^{2-}$ and $[6\text{-Ph-}6,9\text{-}C_2B_8H_9]^{2-}$ with [*cis*-$PtCl_2(PMe_2Ph)_2$] in CH_2Cl_2 yields the yellow crystalline *closo*-structured eleven-vertex compounds [2-X-1,1-$(PMe_2Ph)_2$-1,2,3-$PtC_2B_8H_9$], where X = H (compound **1**), Me (compound **2**), or Ph (compound **3**) in yields of 58 – 88%. These compounds have been characterized by multielement NMR spectroscopy and, in the case of compounds **1** and **2**, by single-crystal X-ray diffraction analysis. Crystals of compound **1** were monoclinic, space group $P2_1/n$, with a = 947.6(1), b = 1 547.7(3), c = 1 804.0(3) pm, β = 104.78(1)°, and Z = 4, solved and refined to R (R_w) = 0.0216 (0.0234) with 4 200 unique reflections $I > 2.0\ \sigma(I)$. Crystals of compound **2** were monoclinic, space group *I2/a* (= *C2/c*), with a = 1 824.8(2), b = 1 016.8(2), c = 1 328.2(3) pm, β = 101.48(2)°, and Z = 4, solved and refined to R (R_w) = 0.0442 (0.0474) with 2 057 unique reflections $I > 2.0\ \sigma(I)$. The NMR and X-ray results reveal that the closed eleven-vertex compounds [2-X-1,1-$(PR_3)_2$-1,2,3-$PtC_2B_8H_9$] exhibit a previously unsuspected but very free contrarotational fluxionality within the constraints of their η^6-carborane-to-metal bonding that is accompanied by a marked flexing of the η^6-$\{C_2B_8H_9X\}$ moiety between *nido* and *arachno* ten-vertex geometries and electronic characteristics. The structural and bonding implications are discussed and elucidated specifically with reference to the NMR and geometrical characteristics of [*closo*-2,3-$C_2B_9H_{11}$], [*arachno*-6,9-$C_2B_8H_{14}$], and the $[nido\text{-}6\text{-X-}6,9\text{-}C_2B_8H_9]^{2-}$ anions, together with other pertinent species such as [μ-6,9-$(SnMe_2)$-*nido*-6,9-$C_2B_8H_{10}$], and more generally with reference to other eleven-vertex metallaheteroborane species. The general behavioural patterns thus established are summarized.

* Contribution No. 24 from the Řež-Leeds Anglo-Czech Polyhedral Collaboration (A.C.P.C.).

**The author to whom correspondence should be addressed.

The ideally C_{2v} deltahedral eleven-vertex cluster configuration *I* is compatible with a continuum of formal Wadian[1] cluster electron counts from *arachno*, as in the [μ-6,9-(PPh_2)-*arachno*-$B_{10}H_{12}$]$^{2-}$ anion[2,3], through *nido*, and then *closo*, as in [μ-6,9-{$Pt(PPh_3)_2$}-*nido*-6,9-$C_2B_8H_{10}$] (refs[4 - 6]) and [1-(η^5-C_5Me_5)-2-Me-*closo*-1,2,3-$RhC_2B_8H_9$] (ref.[7]) to *pileo*, as in the so-called "*isocloso*" species such as [1-(η^5-C_5Me_5)-1-$RhB_{10}H_{10}$] (ref.[8]).

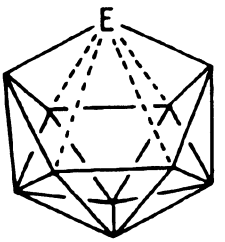

I

Experimental evidence on structural and bonding factors associated with this phenomenon is of interest. Here we report and briefly discuss experimental details on new metalladicarbaborane compounds approximately in the *nido*-type electron-count category near the centre of this continuum. The numbering schemes for the *nido/arachno* ten-vertex, C_{2v} *closo*-type eleven-vertex, and *nido* eleven-vertex clusters encountered in this work are in structures *II* – *IV*, respectively. Note that interconversion among these cluster types can change the formal numbering of a particular atom. Some preliminary aspects of this work have been previously communicated elsewhere[9].

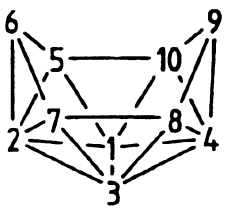

II

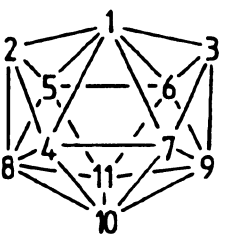

III

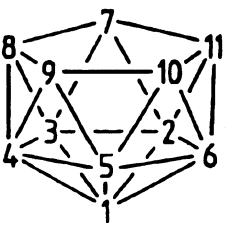

IV

RESULTS AND DISCUSSION

1. Preparation of the Eleven-Vertex Species [1,1-(PMe$_2$Ph)$_2$-1,2,3-PtC$_2$B$_8$H$_9$-2-X], where X = H (Compound 1), Me (Compound 2), and Ph (Compound 3)

Reaction between [*cis*-PtCl$_2$(PMe$_2$Ph)$_2$] and the appropriate [6-X-*nido*-6,9-C$_2$B$_8$H$_9$]$^{2-}$ dianion (X = H, Me, or Ph) in dichloromethane solution at room temperature, followed by chromatographic separation, gave [1,1-(PMe$_2$Ph)$_2$-1,2,3-PtC$_2$B$_8$H$_9$-2-X], where X = H (compound **1**), Me (compound **2**), or Ph (compound **3**), numbering as in structure *III* and Figs 1 and 2. All three were yellow air-stable crystalline solids, yields being 58 – 88%. A simple stoichiometry can be written down for the reactions (Eq. (*A*)), and the basic mechanism can be envisaged as a straightforward displacement of the two chloride anions by the dianionic [XC$_2$B$_8$H$_9$]$^{2-}$ moiety. Exactly analogous routes were used previously[4] to prepare [1,1-(PPh$_3$)$_2$-1, 2,3-PtC$_2$B$_8$H$_{10}$] (compound **4**, see Fig. 3), as well as [1,1-(SEt$_2$)$_2$-1,2,3-PtC$_2$B$_8$H$_{10}$] (compound **5**) and [1,1-(*cis*-1,2-diaminocyclohexane)-1,2,3-NiC$_2$B$_8$H$_{10}$].

$$[PtCl_2(PMe_2Ph)_2] + [XC_2B_8H_9]^{2-} \longrightarrow [(PMe_2Ph)_2PtC_2B_8H_9X] + 2\,Cl^- \qquad (A)$$

1 – 3

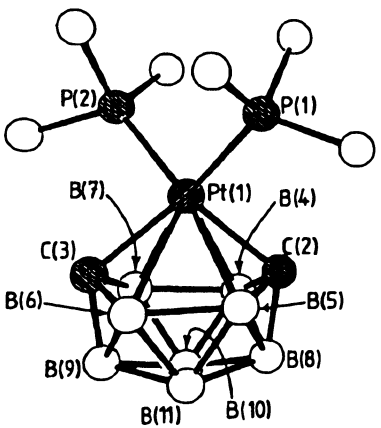

FIG. 1

Crystallographically determined molecular structure of [1,1-(PMe$_2$Ph)$_2$-1,2,3-PtC$_2$B$_8$H$_{10}$] (compound **1**). Hydrogen atoms were not located and P-phenyl carbon atoms (other than the *ipso* ones) are omitted for simplicity. Because of symmetry, in the crystal P(2) = P(1*), C(3) = C(2*), B(6) = B(4*), B(7) = B(5*), B(9) = B(8*), and B(11) = B(10*)

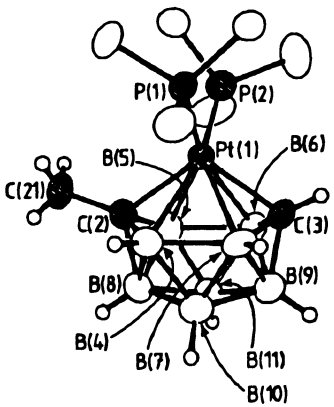

FIG. 2

Crystallographically determined molecular structure of [2-Me-1,1-(PMe$_2$Ph)$_2$-1,2,3-PtC$_2$B$_8$H$_9$] (compound **2**), with P-organyl hydrogen atoms, and P-phenyl carbon atoms (except for the *ipso* ones) omitted for simplicity

The new species **1**, **2**, and **3** were characterized by NMR spectroscopy, as discussed below, and by single-crystal X-ray diffraction analyses on the unsubstituted parent compound **1** and its 2-methyl derivative, compound **2**.

2. Molecular Structures of [1,1-(PMe$_2$Ph)$_2$-1,2,3-PtC$_2$B$_8$H$_{10}$] (Compound 1) and [1,1-(PMe$_2$Ph)$_2$-1,2,3-PtC$_2$B$_8$H$_9$-2-Me] (Compound 2)

Drawings of the crystallographically determined molecular structures of compounds **1** and **2** are in Figs 1 and 2, respectively. Selected nearest neighbour interatomic distances and angles are in Tables I and II, respectively, for compound **1**, and *III* and *IV*, respectively, for compound **2**. All cluster hydrogen atoms were located and refined for the C-methyl compound **2**, but were not locatable crystallographically for compound **1**. However, their presence in compounds **1** is obvious from NMR spectroscopy (see Table VI), confirming the [(PMe$_2$Ph)$_2$PtC$_2$B$_8$H$_{10}$] formulation.

It is apposite to compare the structural details of compounds **1** and **2** with those previously reported for the {Pt(PPh$_3$)$_2$} analogue of compound **1**, viz. [1,1-(PPh$_3$)$_2$-1,2,3-PtC$_2$B$_8$H$_{10}$] (compound **4**). The most marked difference among the three species is that there is a variable twist in the metal-to-carborane bonding. Thus the molecular structures of compound **2** and compound **4** exhibit orthogonally different rotations of the {Pt(PR$_3$)$_2$} moiety with respect to the {C$_2$B$_8$H$_9$X} (X = H for **4** and Me for **2**) dicarbaborane residue (structures *V* and *VII*, respectively, and the outer diagrams in Fig. 3), whereas the rotation in solid-state structure of [(PMe$_2$Ph)$_2$PtC$_2$B$_8$H$_{10}$] (compound **1**) is intermediate (structure *VI* and the centre diagram in Fig. 3).

These different rotations are accompanied by marked differences in the geometry of the {PtC$_2$B$_8$} cluster. Salient distances, together with those of the recently reported[10] main-group analogue [μ-6,9-{Al(OEt$_2$)Et}-*nido*-6,9-C$_2$B$_8$H$_{10}$] (compound **6**) for com-

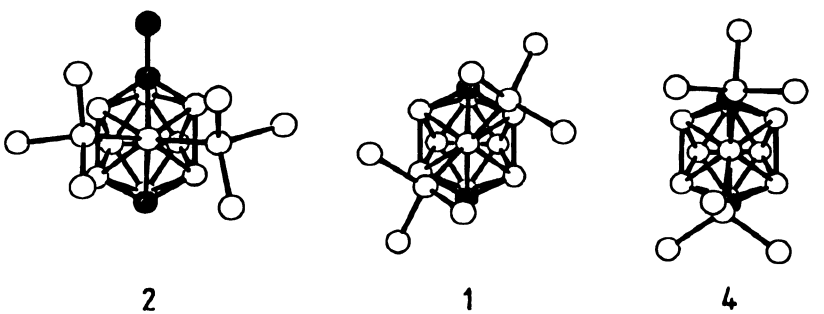

FIG. 3
Drawings of (from left to right) the crystallographically determined solid-state molecular structures of compounds **2** (this work), **1** (this work), and **4** (data from refs[4–6]). The view is chosen to illustrate the rotational twist

parison, are in Table V. For compound **4**, in which the two ligand phosphorus atoms eclipse the carbon atoms in the 2- and 3-positions, the platinum is much further out of the cluster (structure *VIII*). This molecular structure has been interpreted[4,5] in terms of a square-planar platinum(II) moiety simply bridging the 6,9-positions of the *nido*-type $\{6,9\text{-}C_2B_8H_{10}\}$ residue. Such a simple bridging would be as found, for example, in main group analogues such as the aluminium compound **6**, although detailed NMR

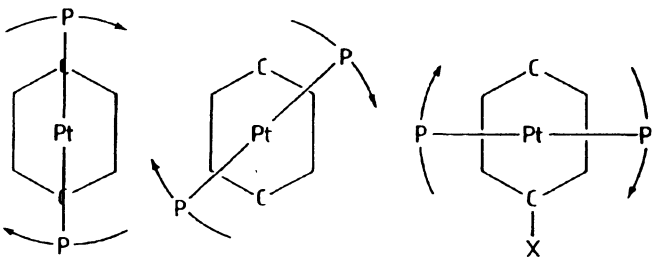

V *VI* *VII*

TABLE I

Selected interatomic distances (in pm) for $[1,1\text{-}(PMe_2Ph)_2\text{-}1,2,3\text{-}PtC_2B_8H_{10}]$ (**1**) with estimated standard deviations (e.s.d.'s) in parentheses[a]

Atoms	Distance	Atoms	Distance
P(1)–Pt(1)	226.7(4)	C(2)–Pt(1)	215.5(10)
B(4)–Pt(1)	257.2(13)	B(5)–Pt(1)	243.4(13)
C(11)–P(1)	184.1(12)	C(12)–P(1)	182.5(12)
C(131)–P(1)	181.5(12)		
C(132)–C(131)	140(2)	C(136)–C(131)	140.0(14)
C(133)–C(132)	141(2)	C(134)–C(133)	141(2)
C(135)–C(134)	137(2)	C(136)–C(135)	139(2)
B(4)–C(2)	161(2)	B(4)–B(8)	183(2)
B(5)–C(2)	155(2)	B(4)–B(10)	178(2)
B(8)–C(2)	159(2)		
B(5)–B(6*)	190(3)	B(8)–B(10)	177(2)
B(5)–B(8)	181(2)	B(9*)–B(10)	177(2)
B(10)–B(5)	182(2)	B(10)–B(11*)	185(4)

[a] The following atom pairs are related by a two-fold rotation axis (C_2) using the symmetry operation (1.5 – *x*), (*y*), (–*z*): P(1) and P(1*), C(2) and C(3*), B(4) and B(6*), B(5) and B(7*), B(8) and B(9*), B(10) and B(11*), P(1*) = P(2) in Fig. 1.

considerations (see Section *4* below) now suggest that an overall electronic structure similar to that of eleven-vertex [*closo*-2,3-$C_2B_9H_{11}$] might be a better approximation for the platinum compound **4**. (Note that because of the tetrahedral, as distinct from square-planar, bonding about the aluminium atom, compound **6** exhibits an approximately orthogonal rotation of its *exo*-cluster ligand sphere relative to that exhibited by **4**). For compound **2**, by contrast, the platinum atom is held much more compactly in the cluster (structure *IX*), and it is now within much closer bonding distance of the four boron atoms. In this more compact cluster, these platinum–boron distance of 237.5(7) – 240.2(7) pm are towards the higher end of previously observed platinum–boron distances[11,12] for reasonable bonding interactions in polyhedral boron-containing com-

TABLE II
Selected interatomic angles (in °) for [1,1-$(PMe_2Ph)_2$-1,2,3-$PtC_2B_8H_{10}$] (**1**) with e.s.d.'s in parentheses[a]

Atoms	Angle	Atoms	Angle
P(1)–Pt(1)–P(1*)	91.5(2)	C(2)–Pt(1)–P(1)	149.9(3)
C(2)–Pt(1)–P(1*)	92.8(4)	C(2)–Pt(1)–C(3*)	98.1(4)
B(4)–Pt(1)–P(1)	118.7(4)	B(4)–Pt(1)–P(1*)	124.8(4)
B(4)–Pt(1)–C(2)	38.5(3)	B(4)–Pt(1)–C(3*)	78.2(4)
B(5)–Pt(1)–P(1)	169.1(3)	B(5)–Pt(1)–P(1*)	94.2(4)
B(5)–Pt(1)–C(2)	39.0(4)	B(5)–Pt(1)–C(3*)	77.6(5)
B(5)–Pt(1)–B(4)	64.9(5)	B(5)–Pt(1)–B(6*)	44.4(4)
B(5)–Pt(1)–B(7*)	81.7(5)		
B(4)–C(2)–Pt(1)	84.9(6)	B(5)–C(2)–Pt(1)	80.3(6)
B(5)–C(2)–B(4)	116.5(9)	B(8)–C(2)–Pt(1)	125.0(8)
B(8)–C(2)–B(4)	69.7(10)	B(8)–C(2)–B(5)	70.7(11)
C(2)–B(4)–Pt(1)	56.6(5)	B(7*)–B(4)–Pt(1)	64.0(6)
B(7*)–B(4)–C(2)	110.6(9)	B(8)–B(4)–Pt(1)	97.1(8)
B(8)–B(4)–C(2)	54.8(8)	B(8)–B(4)–B(7*)	105.2(9)
B(10)–B(4)–Pt(1)	105.1(8)	B(10)–B(4)–C(2)	105.1(10)
B(10)–B(4)–B(7*)	59.5(8)	B(10)–B(4)–B(8)	58.7(9)
C(2)–B(5)–Pt(1)	60.8(6)	B(6*)–B(5)–Pt(1)	71.7(6)
B(6*)–B(5)–C(2)	120.4(10)	B(8)–B(5)–Pt(1)	102.6(9)
B(8)–B(5)–C(2)	56.0(8)	B(8)–B(5)–B(6*)	107.5(10)
B(11*)–B(5)–Pt(1)	109.1(9)	B(11*)–B(5)–C(2)	106.9(10)
B(11*)–B(5)–B(6*)	57.0(8)	B(11*)–B(5)–B(8)	58.5(9)

[a] The following atom pairs are related by a two-fold rotation axis (C_2) using the symmetry operator (1.5 – *x*), (*y*), (–*z*): P(1) and P(1*); P(1*) ≡ P(2), C(2) and C(3*), B(4) and B(6*), B(5) and B(7*), B(8) and B(9*), B(10) and B(11*).

TABLE III
Selected interatomic distances (in pm) for [1,1-$(PMe_2Ph)_2$-1,2,3-$PtC_2B_8H_9$-2-Me] (**2**) with e.s.d.'s in parentheses

Atoms	Distance	Atoms	Distance
P(1)–Pt(1)	228.8(3)	P(2)–Pt(1)	228.8(3)
C(3)–Pt(1)	217.6(6)	C(2)–Pt(1)	218.6(6)
B(4)–Pt(1)	238.4(7)	B(5)–Pt(1)	237.7(7)
B(6)–Pt(1)	237.5(7)	B(7)–Pt(1)	240.2(7)
C(21)–C(2)	152.0(8)	H(21a)–C(21)	88.2(56)
H(21b)–C(21)	112.2(75)	H(21c)–C(21)	96.8(63)
C(2)–B(4)	157.9(9)	C(3)–B(6)	156.7(8)
C(2)–B(5)	156.8(9)	C(3)–B(7)	155.2(9)
C(2)–B(8)	166.6(8)	C(3)–B(9)	163.8(8)
B(4)–B(5)	257.0(11)	B(5)–B(6)	198.8(9)
B(4)–B(7)	197.4(9)	B(5)–B(8)	180.5(10)
B(4)–B(8)	179.3(10)	B(5)–B(11)	181.0(9)
B(4)–B(10)	179.2(9)		
B(6)–B(7)	259.1(10)	B(7)–B(9)	181.6(9)
B(6)–B(9)	180.9(9)	B(7)–B(10)	179.7(9)
B(6)–B(11)	180.1(9)		
B(8)–B(10)	173.3(10)	B(9)–B(10)	175.6(9)
B(8)–B(11)	175.3(9)	B(9)–B(11)	174.6(9)
B(10)–B(11)	184.6(10)		
H(3)–C(3)	74(5)	H(8)–B(8)	104(4)
H(4)–B(4)	110(4)	H(9)–B(9)	114(4)
H(5)–B(5)	109(5)	H(10)–B(10)	118(4)
H(6)–B(6)	110(5)	H(11)–B(11)	99(4)
H(7)–B(7)	106(4)		
C(2)..C(3)	352.1(8)		
B(6)..B(7)	259.1(8)	B(4)..B(5)	257.0(9)
Pt(1) to C(2)..C(3) vector	129.3(3)		
Pt(1) to B(4)B(5)B(6)B(7) plane	174.3(2)		

TABLE IV
Selected interatomic angles (in °) for [1,1-$(PMe_2Ph)_2$-1,2,3-$PtC_2B_8H_9$-2-Me] (**2**) with e.s.d.'s in parentheses

Atoms	Angle	Atoms	Angle
P(2)–Pt(1)–P(1)	94.3(1)	C(3)–Pt(1)–P(1)	115.8(2)
C(3)–Pt(1)–P(2)	109.8(2)	C(2)–Pt(1)–P(1)	111.7(2)
C(2)–Pt(1)–P(2)	118.1(2)	C(2)–Pt(1)–C(3)	107.2(3)
B(4)–Pt(1)–P(1)	95.4(2)	B(4)–Pt(1)–P(2)	158.2(1)
B(4)–Pt(1)–C(3)	83.3(3)	B(4)–Pt(1)–C(2)	40.1(2)
B(5)–Pt(1)–P(1)	151.2(1)	B(5)–Pt(1)–P(2)	97.8(2)
B(5)–Pt(1)–C(3)	84.4(3)	B(5)–Pt(1)–C(2)	39.9(2)
B(5)–Pt(1)–B(4)	65.3(3)	B(6)–Pt(1)–P(1)	155.5(1)
B(6)–Pt(1)–P(2)	93.3(2)	B(6)–Pt(1)–C(3)	40.0(2)
B(6)–Pt(1)–C(2)	84.9(3)	B(6)–Pt(1)–B(4)	85.9(3)
B(6)–Pt(1)–B(5)	49.5(2)	B(7)–Pt(1)–P(1)	97.0(2)
B(7)–Pt(1)–P(2)	148.5(1)	B(7)–Pt(1)–C(3)	39.3(2)
B(7)–Pt(1)–C(2)	84.6(3)	B(7)–Pt(1)–B(4)	48.7(2)
B(7)–Pt(1)–B(5)	86.1(3)	B(7)–Pt(1)–B(6)	65.7(3)
C(21)–C(2)–Pt(1)	123.4(4)	B(4)–C(2)–Pt(1)	76.7(3)
B(4)–C(2)–C(21)	124.2(6)	B(5)–C(2)–Pt(1)	76.6(3)
B(5)–C(2)–C(21)	125.1(6)	B(5)–C(2)–B(4)	109.5(5)
B(8)–C(2)–Pt(1)	114.6(4)	B(8)–C(2)–C(21)	121.9(5)
B(8)–C(2)–B(4)	67.0(4)	B(8)–C(2)–B(5)	67.7(4)
B(6)–C(3)–Pt(1)	76.9(3)	B(7)–C(3)–Pt(1)	78.2(3)
B(7)–C(3)–B(6)	112.4(5)	B(9)–C(3)–Pt(1)	117.2(4)
B(9)–C(3)–B(6)	68.7(4)	B(9)–C(3)–B(7)	69.3(4)
H(3)–C(3)–Pt(1)	122.4(38)	H(3)–C(3)–B(6)	120.2(39)
H(3)–C(3)–B(7)	126.4(39)	H(3)–C(3)–B(9)	120.2(38)
C(2)–B(4)–Pt(1)	63.2(3)	B(5)–B(4)–Pt(1)	57.2(3)
B(5)–B(4)–C(2)	35.1(2)	B(7)–B(4)–Pt(1)	66.1(3)
B(7)–B(4)–C(2)	120.5(4)	B(7)–B(4)–B(5)	90.8(4)
B(8)–B(4)–Pt(1)	101.4(4)	B(8)–B(4)–C(2)	58.8(4)
B(8)–B(4)–B(5)	44.6(2)	B(8)–B(4)–B(7)	105.2(4)
B(10)–B(4)–Pt(1)	105.0(4)	B(10)–B(4)–C(2)	110.3(5)
B(10)–B(4)–B(5)	78.6(4)	B(10)–B(4)–B(7)	56.7(4)
B(10)–B(4)–B(8)	57.8(4)		
C(2)–B(5)–Pt(1)	63.5(3)	B(4)–B(5)–Pt(1)	57.5(3)
B(4)–B(5)–C(2)	35.4(2)	B(6)–B(5)–Pt(1)	65.2(3)
B(6)–B(5)–C(2)	119.7(5)	B(6)–B(5)–B(4)	89.8(4)
B(8)–B(5)–Pt(1)	101.3(4)	B(8)–B(5)–C(2)	58.7(4)
B(8)–B(5)–B(4)	44.2(2)	B(8)–B(5)–B(6)	104.6(5)

TABLE IV
(*Continued*)

Atoms	Angle	Atoms	Angle
B(11)–B(5)–Pt(1)	104.7(4)	B(11)–B(5)–C(2)	110.4(5)
B(11)–B(5)–B(4)	78.4(4)	B(11)–B(5)–B(6)	56.4(4)
B(11)–B(5)–B(8)	58.0(4)		
C(3)–B(6)–Pt(1)	63.1(3)	B(5)–B(6)–Pt(1)	65.3(3)
B(5)–B(6)–C(3)	118.5(4)	B(7)–B(6)–Pt(1)	57.6(2)
B(7)–B(6)–C(3)	33.6(2)	B(7)–B(6)–B(5)	89.9(4)
B(9)–B(6)–Pt(1)	101.8(4)	B(9)–B(6)–C(3)	57.5(4)
B(9)–B(6)–B(5)	105.0(4)	B(9)–B(6)–B(7)	44.5(2)
B(11)–B(6)–Pt(1)	105.0(4)	B(11)–B(6)–C(3)	108.6(5)
B(11)–B(6)–B(5)	56.8(4)	B(11)–B(6)–B(7)	78.2(4)
B(11)–B(6)–B(9)	57.9(4)		
C(3)–B(7)–Pt(1)	62.5(3)	B(4)–B(7)–Pt(1)	65.2(3)
B(4)–B(7)–C(3)	118.3(4)	B(6)–B(7)–Pt(1)	56.7(3)
B(6)–B(7)–C(3)	34.0(2)	B(6)–B(7)–B(4)	89.5(4)
B(9)–B(7)–Pt(1)	100.6(4)	B(9)–B(7)–C(3)	57.6(4)
B(9)–B(7)–B(4)	104.9(4)	B(9)–B(7)–B(6)	44.3(2)
B(10)–B(7)–Pt(1)	104.1(4)	B(10)–B(7)–C(3)	108.8(5)
B(10)–B(7)–B(4)	56.5(4)	B(10)–B(7)–B(6)	78.0(4)
B(10)–B(7)–B(9)	58.2(4)		
B–B–C (obtuse)	106.9(4) – 110.4(5)	B–B–C (acute)	53.1(4) – 58.8(4)
B–B–B (obtuse)	104.6(5) – 106.1(4)	B–B–B (acute)	56.4(4) – 64.1(4)
Dihedral angles			
P(1)P(2)Pt(1)/Pt(1)B(10)B(11)	5.4(2)		
P(1)P(2)Pt(1)/Pt(1)C(2)C(3)	85.2(2)		

pounds, although it should be pointed out that longer distances are dictated geometrically for this capped-boat deltahedral shape: for example, the platinum–boron and platinum–carbon distances in **2** are, in fact, very similar to the corresponding distances[7] to rhodium in the more conventional *closo*-type eleven-vertex compound [1-(η^5-C_5Me_5)-2-Me-*closo*-1,2,3-$RhC_2B_8H_9$]. However, the corresponding metal–boron distances in the more expanded cluster of compound **4**, of 258(1) – 266(1) pm, clearly indicate much weaker interactions[5].

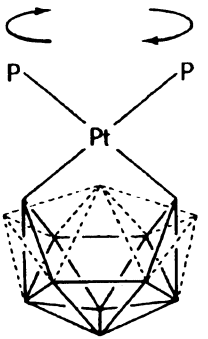

VIII

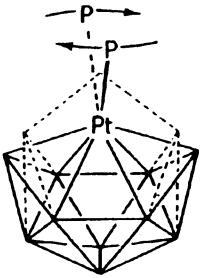

IV

TABLE V
Selected interatomic distances (in pm) and angles (in °) for the platinadicarbaboranes **1**, **2**, and **4**, and for the aluminadicarbaborane **6**

Dimension	**2**	**1**	**4**[a]	**6**[b]
C(2)–C(3)	351.2(6)	325.4(14)	316.2(13)	309.4
B(4)–B(5)	257.0(7)	268.7(16)	265.0(14)	265.3
B(6)–B(7)	259.0(7)	268.7(16)	269.0(15)	264.1
P(1)Pt(1)P(2)/C(2)C(3)	85.2(2)	48.9(2)	6.2(2)	[87.9][b]
Pt(1) from C(2)C(3)	129.3(2)	141.3(1)	145.4(1)	[131.1][b]
C(2) from B(4)B(5)B(6)B(7)	46.0(4)	48.2(9)	57.0(8)	59.3
C(3) from B(4)B(5)B(6)B(7)	44.0(4)	48.2(9)	62.1(7)	59.1
C(2)–Pt(1)–C(3)	107.2(3)	98.1(3)	94.8(3)	[99.4][b]
P(1)–Pt(1)–P(2)	94.3(1)	93.5(1)	93.7(2)	[99.9]

[a] Calculated from coordinates in ref.[7]. [b] Calculated from coordinates in ref.[11]; for Pt substitute Al and for the phosphines substitute OEt_2 and ethyl.

These platinum bonding differences are also accompanied by a marked fundamental flexing of the $\{C_2B_8\}$ residue itself (structures *VIII* and *IX* and Table V), manifested principally in a 35(2) pm change in the C(2)...C(3) non-bonded distance from 316.2(13) pm in compound **4** to 351.2(6) pm in compound **2**. This corresponds to an extreme change from *nido* to *arachno* in the $\{C_2B_8\}$ ten-vertex geometry (the corresponding $[B_{10}H_{14}]/[B_{10}H_{14}]^{2-}$ difference[13,14] being ca 18 pm); this *nido* versus *arachno* character difference tends to be supported by the NMR considerations discussed below in Section *4*. The half-twist distortions observed for compound **1** are nicely intermediate, confirming that these interesting structural differences among compounds **1**, **2** and **4** are not artefacts arising from the crystallographic analysis itself.

Although the steric effect of the C-methyl group in compound **2** will have some role in dictating the observed solid-state phosphine configuration, the very ready rotational fluxionality about platinum of these species (see Section *4* below and arrows in structures *V – IX*) suggests that the observed solid-state configurations may not necessarily correspond to the minimum-energy fluid-state rotamers. Indeed, in a general context it should be noted that in suitable cases fluxionality can also in principle occur in the solid-state on the NMR (as distinct from X-ray) time-scale. This is unlikely in this instance, but it would nevertheless be interesting to compare the (traces of) the ^{11}B chemical shift tensors in the solid-state for compounds **1** and **2**, because the geometrical differences do imply marked bonding differences. The NMR considerations summarized below (Section *4*) in fact suggest that the fluid-state minimum-energy rotamer for the two $\{Pt(PMe_2Ph)_2\}$ species **1** and **2** (and also thereby the C-phenyl derivative **3**) approximate to the solid-state structure observed for compound **2** (i.e. structures *VII* and *IX*), whereas that for the $\{Pt(PPh_3)_2\}$ compound **4** [and also the $\{Pt(SEt_2)_2\}$ species **5**] must be close to that observed[4-6] in the solid-state for **4** (i.e. structures *V* and *VIII*). As mentioned in our preliminary note[9], it is of interest that simple exchange of PPh_3 for PMe_2Ph on platinum can induce such a gross change in the platinum-to-cluster bonding character. The differences in electronic energy between these two forms must therefore be small, and, for the unsubstituted $\{Pt(PMe_2Ph)_2\}$ compound **1** in particular (see Section *4* below), it is reasonably presumed that the free-energy barrier to fluxional rotation is therefore very low indeed[9], and that the half-twist observed for **1** in the solid-state (structure *VI* and Fig. 3, centre plot) arises from the dominance of crystal-packing forces over at least the initial foothills of this rotational barrier.

3. Cluster Geometry and Electron-Counting Considerations in the Closed {1,2,3-PtC2B8} Types of Systems

Compounds **1 – 5** are of interest because they have closed deltahedral C_{2v} structures as expected for *closo*[15] eleven-vertex systems, but can in some respects be considered to have formal *nido* (ref.[1]) cluster electron counts. Thus, if the $\{Pt(PR_3)_2\}$ moieties are considered in the first instance as part of approximately square planar (compound **4**), or

possibly tetrahedral (compound **2**) platinum(II) bonding systems, then the cluster structures can be considered analogous to that of a ten-vertex $\{nido\text{-}6,9\text{-}C_2B_8H_{10}\}^{2-}$ moiety (numbering as in *II* above) bridged across the 6,9-positions with a $\{BH_2\}^+$ group, i.e. as $[C_2B_9H_{12}]^-$ equivalents. In this case the formal bidentate $\{C_2B_8H_{10}\}^{2-}$ ligand on $\{Pt(PR_3)_2\}^{2+}$ would be expected to maintain *nido* character, which is somewhat in accord with the geometric considerations for the $\{Pt(PPh_3)_2\}$ and $\{Pt(SEt_2)_2\}$ species **4** and **5** (Section *2*), but somewhat at variance with NMR considerations (Section *4* below). Alternatively, (and particularly in view of the stronger Pt(1) interaction with B(4)B(5)B(6)B(7) in the $\{P(PMe_2Ph)_2\}$ (compound **2**), if, in addition to the foregoing, additional platinum-to-boron bonding and thence platinum(IV) character[16 - 18] is invoked, then the structures can be considered analogous to a ten-vertex $\{nido\text{-}6,9\text{-}C_2B_8H_{10}\}^{2-}$ moiety capped by a neutral {BH} unit that contributes three orbitals and two electrons to the eleven-vertex cluster bonding proper, i.e. as $[C_2B_9H_{11}]^{2-}$ equivalents. In this case in metal complex terms the *nido* $\{C_2B_8H_{10}\}^{2-}$ anion would thereby gain two electrons from the metal centre and consequently acquire the formal character of an *arachno* $\{C_2B_8H_{10}\}^{4-}$ ligand tetradentate to $\{Pt(PR_3)_2\}^{4+}$ which is in accord with the geometric and NMR considerations for compounds **1** and **3** as discussed in Sections *2* above and *4* below. In either case, both $[C_2B_9H_{12}]^-$ and $[C_2B_9H_{11}]^{2-}$ are formal *nido* formulations (refs[1,15]).

A third useful approach is to consider the compounds as complexes between the η-$\{nido\text{-}C_2B_8H_{10}\}^{2-}$ ligand and a $\{Pt(PR_3)_2\}^{2+}$ unit that contributes an additional vertex and no extra electrons to the cluster bonding and thus effects a classical[1,15] ten-vertex → eleven-vertex *nido* → *closo* conversion. This would certainly be consistent with the observed *closo*-type structures, and consistent with the marked NMR similarities of compounds **4** and **5** to $[closo\text{-}2,3\text{-}C_2B_9H_{11}]$ itself, to which, in this model, they would be equivalent. In these terms the capping $\{Pt(PR_3)_2\}^{2+}$ vertex would be regarded as a $\{BH\}^{2+}$ equivalent (rather than as a $\{BH_2\}^+$ equivalent as discussed for the 6,9-bridging model above), which contributes three orbitals (rather than two in the $\{BH_2\}^{2+}$ model) to the cluster bonding proper. This three-orbital model implies some acceptance, by the formal $\{Pt(PR_3)_2\}^{2+}$ metal centre, of electron density from the B(4)B(7)/B(5)B(6) region as well as from C(2) and C(3). In metal complex terms this model would imply a formal platinum(II) complex between a tridentate $\{nido\text{-}C_2B_8H_{10}\}^{2-}$ moiety and the $\{Pt(PR_3)_2\}^{2+}$ centre. However, the longer platinum-to-boron distances in compound **4**, as discussed in the next paragraph, suggest that the boron-to-metal donation would not necessarily be particularly strong.

In purely geometric terms, the long platinum-to-boron distances in the less compact cluster of the $\{Pt(PPh_3)_2\}$ compound **4** could suggest that irrespective of any electronic considerations, any supposed attempt by the cluster to accommodate a more open *nido* character may be provided by a symmetrical "slippage" of the platinum atom away from the cluster, as manifested in an equal expansion of the two five-membered convex

faces defined by Pt(1)C(2)C(3)B(4)B(7) and Pt(1)C(2)C(3)B(5)B(6). If asymmetry were present, as it is in the conventionally *nido*-structured isoelectronic quasi-isomer [10,10-$(PMe_3)_2$-*nido*-10,7,9-$PtC_2B_8H_{10}$] (refs[19,20]), (Fig. 4), then asymmetric opening to give one well-defined open face would probably be induced (see Section *5* below. The compound is believed to be fluxional in solution via a pentagonal-belt-rotational mechanism that averages certain ^{11}B environments on the NMR time-scale, but in which the two ^{31}P resonances remain distinct (contrast mechanism for compounds **1**, **2**, and **3**).

By contrast, the cluster structure of the $\{Pt(PMe_2Ph)_2\}$ species **2** is much more compact than that of **4**, with no significant suggestion of slippage, which shows that other factors operate. As discussed in the previous paragraphs it seems likely that the compactness arises from increased platinum-to-boron bonding-electron density. This thereby constitutes an interesting example of increased electron donation to a boron-containing cluster from a cluster constituent itself, that produces a more tightly bound and compact cluster. Conventionally an increased electron donation results in cluster opening.

It is also apparent from the observed fluxionality of compounds **2** and **3** (and by implication **1**, and possibly, **4** and **5**) (Section *4* below), that all three of the compact (compound **2**), expanded (compound **4**) and intermediate (compound **1**) forms of these $\{1,2,3\text{-}PtC_2B_8H_{10}\}$ clusters are energetically very similar. It is also of interest that in these species the formal *nido* 26-electron count can be accommodated by these symmetrical, formally *closo*, eleven-vertex geometries, whereas, conversely, in the eleven-vertex formal *closo* 24-electron system, the *closo* structures themselves are often uncomfortable, and there is often a tendency for *nido*-type open faces to occur (see, for example, ref.[21] and Section *5* below).

It will be of interest to have some rigorous quantum mechanical work to help understand the bonding in these eleven-vertex systems (see also Section *5* below). Mean-

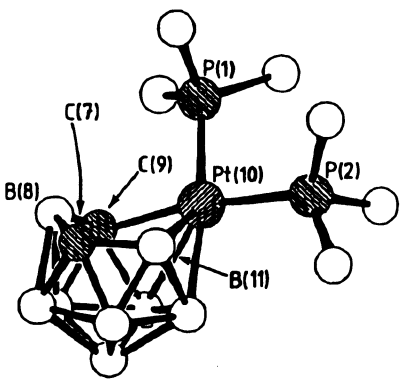

FIG. 4
Crystallographically determined molecular structure of the *nido*-shaped cluster compound [10,10-$(PMe_3)_2$-10,7,9-$PtC_2B_8H_{10}$] (data from refs[19,20]). In cluster terms this is isoelectronic with compounds **1**, **2**, and **4** (e.g. Figs 1, 2, and 3) which have *closo*-shaped clusters

while, since NMR chemical shifts and coupling constants depend intimately upon electronic structure, we thought it of some empirical use to examine the NMR behaviour of compound **1**, **2**, and **3**, and of other species containing {*nido*/*arachno*-6,9-C_2B_8} types of fragment, to compare for parallels in NMR behaviour that may indicate bonding similarities.

4. Comparative Nuclear Magnetic Resonance Studies

The measured NMR parameters for the {$Pt(PMe_2Ph)_2$} compounds **1**, **2**, and **3** are included in Tables VI and VII, and these data, together with the additional experimental evidence summarized, were sufficient to assign the ^{11}B and ^1H NMR chemical shifts to the individual cluster positions in each compound. Also in Table VI are the available data for the {$Pt(PPh_3)_2$} and {$Pt(SEt_2)_2$} compounds **4** and **5**. The top diagram in Fig. 5 plots $\delta(^1H)$ versus $\delta(^{11}B)$ for the individual {BH} units of compounds **1** – **4**, and it is interesting that the gradient of this plot, at $\delta(^1H) : \delta(^{11}B)$ ca 1 : 8 with intercept +3.00 in $\delta(^1H)$, is much steeper than has generally been found for straightforward *nido* and *arachno* species (see, for example, refs[22 – 24]), perhaps reflecting in some way the unusual structure-electronic factors discussed in Sections *3* and *5*.

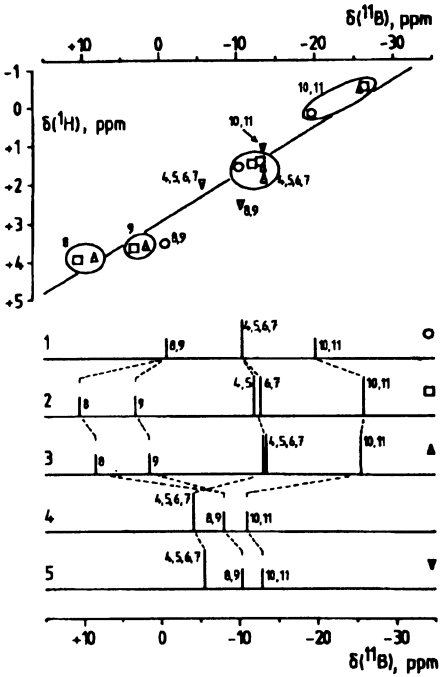

FIG. 5
Proton and boron-11 NMR data for compounds **1**, **2**, **3**, **4**, and **5**. The top diagram is a plot of $\delta(^1H)$ versus $\delta(^{11}B)$ for directly bound {BH(*exo*)} atoms for compounds **1**, **2**, **3**, and **5**

TABLE VI

Measured NMR properties for $[(PMe_2Ph)_2PtC_2B_8H_9Me]$ (**2**), $[(PMe_2Ph)_2PtC_2B_8H_9Ph]$ (**3**), $[(PMe_2Ph)_2PtC_2B_8H_{10}]$ (**1**), $[(SMe_2)_2PtC_2B_8H_{10}]$ (**5**), and $[(PPh_3)_2PtC_2B_8H_{10}]$ (**4**) in CD_2Cl_2 solution at 294 – 297 K

Assignment[a] or alternative parameter	**2**		**3**		**1**		**5**		**4**
	$\delta(^{11}B)$	$\delta(^1H)$[b]	$\delta(^{11}B)$	$\delta(^1H)$	$\delta(^{11}B)$	$\delta(^1H)$	$\delta(^{11}B)$	$\delta(^1H)$	$\delta(^{11}B)$
10, 11	−26.2	−0.53	−25.7	−0.47	−19.9	+0.15	−13.3	+1.15	−10.7
8	+10.6	+3.90[c]	+8.6	+3.87[d]	−0.8	+3.50[e]	−10.4	+2.59[f]	−7.8
9	+1.5	+3.66[g]	+3.2	+3.69[h]					
4,5	−12.0	+1.51	~ −13.5	+1.54	−10.3	−1.60	−5.07	+2.02	−3.9
6,7	−12.8	+1.45	~ −13.5	+1.83					
2	[CMe]	+3.16[i]	[CPh]	[j]	[CH]	+4.72	[CH]	+3.19[k]	–
3	[CH]	+4.92[l]	[CH]	+5.09[m]					
$\delta(^1H)(PMe_2)$ $[^3J(^{195}Pt\text{-}^1H)]$ $[N(^{31}P\text{-}^1H)]$[q]	+1.25[25.4]{~ 10.7}[n] −1.33[25.4]{~ 11.3}[n]		+1.39[25.4]{10.7}[o] +1.58[26.4]{11.2}[o]		+1.63[28.6]{10.3}		$[CH_3$ 1.26, CH_2 2.82$]^p$		–
$\delta(^{31}P)$	−24.9		−24.7		−22.3		–		+15.0
$\delta(^{195}Pt)$	−798		−708		−871		[j]		
$^1J(^{195}Pt\text{-}^{31}P)$	(+)3 584		(+)3 582		(+)3 542		–		(+)3 594

[a] Assignments by incidence of satellites, relative intensities, increase of multiplicity upon substitution, $[^1H\text{-}^1H]$-COSY on compound **2**, and intercomparison among the compounds. [b] For $[^1H\text{-}^1H]\{^{11}B\}$-COSY information see Table VII. [c] $^3J(^{195}Pt\text{-}^1H) = 91$ Hz. [d] $^3J(^{195}Pt\text{-}^1H) = 93$ Hz. [e] $^3J(^{195}Pt\text{-}^1H) \approx 80$ Hz. [f] $^3J(^{195}Pt\text{-}^1H) = 88$ Hz. [g] $^3J(^{195}Pt\text{-}^1H) = 103$ Hz. [h] $^3J(^{195}Pt\text{-}^1H) = 103$ Hz. [i] $^3J(^{195}Pt\text{-}^1H) = 26$ Hz; $\delta(^1H)(CD_3C_6D_5) = +3.51$. [j] Not measured. [k] $^3J(^{195}Pt\text{-}^1H) = 34$ Hz. [l] $^3J(^{195}Pt\text{-}^1H) = 27$ Hz; $\delta(^1H)(CD_3C_6D_5) = +5.27$. [m] $\delta(^1H)(CD_3C_6D_5) = +5.38$. [n] These values are for $CD_3C_6D_5$ solution at 231 K: coalescence temperature ($CD_3C_6D_5$ solution) 284 K at 2.35 Tesla; $\Delta\nu$(extrapolated) 7.4 Hz at 284 K; resonances not differentiated in CD_2Cl_2 or $CDCl_3$ solution at low temperatures; $\delta(^1H)(CDCl_3)$ +1.54 at 294 K. [o] In $CD_3C_6D_5$ solution these have values of +1.19 and +1.44 at 294 K; coalescence temperature ($CD_3C_6D_5$ solution) 385 K at 2.35 Tesla; $\Delta\nu$ (extrapolated) 22.4 Hz at 385 K. [p] $N(^{31}P\text{-}^1H) = [^2J(^{31}P\text{-}^1H) + {}^4J(^{31}P\text{-}^1H)]$. [q] Refers to SEt_2 group; the CH_2 group in fact consisted of two resonance patterns differing in $\delta(^1H)$ by ca 0.007 ppm arising from the prochirality of the α-carbon.

The lower diagrams in Fig. 5 compare the chemical shifts and relative intensities among the ^{11}B spectra of compound **1** and its C(2)-substituted analogues **2** and **3**. The $\{Pt(PPh_3)_2\}$ and $\{Pt(SEt_2)_2\}$ compounds **4** and **5** are also included for comparison. Hatched lines join equivalent positions. Note the similarities among compounds **1**, **2**, and **3**, and between **4** and **5**, and the differences between these two sets of compounds. Among **1** – **3** the largest shielding changes are negative substituent effects at the $^{11}B(8)$ positions adjacent (α) to the substituted C(2) atoms, the only other marked effects being the β upfield shifts of $^{11}B(10,11)$ upon C(2) substitution, the other cluster ^{11}B changes being trivial. Apart from these straightforward substituent effects there are no marked differences, which suggests that the minimum-energy fluid-state rotamers do not differ greatly among compounds **1**, **2**, and **3**. The steric effects of the C-methyl and C-phenyl groups in compounds **2** and **3** will force a minimum-energy configuration that is close to that observed in the solid-state for compound **2**, implying that the observed solid-state differences between compounds **1** and **2** derive principally from crystal-packing forces that induce the observed solid-state rotation in **1**. As mentioned above, a solid state comparison of the resultants of the ^{11}B NMR chemical shift tensors in **1** and **2** in the crystalline solid state would be of interest in this context.

The mutually similar ^{11}B data for compounds **4** and **5** in Fig. 5, however, reveal a different shielding pattern, and suggest that the fluid-state minimum-energy configurations of **4** and **5** are also mutually similar, but different from those of compounds **1** – **3**. It is probable[9] that this minimum-energy configuration of **4** and **5** is very similar to that observed[5,6] in the solid-state for compound **4**.

In this context it is useful to compare these shielding patterns with other molecules containing the *nido/arachno*-shaped $\{6,9\text{-}C_2B_8\}$ fragment (structure *II*). As part of this work we have therefore measured and assigned the ^{11}B and ^{1}H shielding patterns for the *nido* species $[6\text{-R-}6,9\text{-}C_2B_8H_9]^{2-}$ (R = H, Me, and Ph) (data in Table VIII), and for the *closo* species $[2,3\text{-}C_2B_9H_{11}]$ (data in Table IX). Figure 6 contains stick repre-

TABLE VII
Observed $[^1H\text{-}^1H]$-COSY correlations for $[(PMe_2Ph)PtC_2B_8H_9Me]$ (**2**); CD_2Cl_2 solution at 297 K

Assignment	$\delta(^1H)$	Observed correlations[a]
3	+4.92	6,7 s; 9 s
4,5	+1.51	8 m; 10,11 w
6,7	+1.45	3 s; 9 w; 10,11 m
8	+3.90	4,5 m; 10,11 s
9	+3.66	3 s; 9 w; 10,11 s
10,11	−0.53	4,5 w; 6,7 m; 8 s; 9 s

[a] s strong, w weak, m medium.

sentations of the assigned chemical shifts and relative intensities in the ^{11}B NMR spectra of compounds **1** and **5**, together with analogous data for the unmetallated *arachno* and *nido* ten-vertex models [*arachno*-6,9-$C_2B_8H_{14}$] (ref.[25]) and the [*nido*-6,9-$C_2B_8H_{10}]^{2-}$ anion. Hatched lines join equivalent positions in the six compounds. Note the similarities between A and B, between C and D, and between E and F, and the gradual progression from *arachno* to *nido* ten-vertex character in the sequence A, B → C, D → E, F. Also included are data for [*closo*-2,3-$C_2B_9H_{11}$] and for the recently reported[26] compound (μ-6,9-($SnMe_2$)-*nido*-6,9-$C_2B_8H_{10}$] (reported data[26] summarized in Table X for convenience of reference; numbering as in structure *II*). This last μ-6,9-dimethylstannadicarbaborane is reasonably presumed analogous to the structurally characterized[10] aluminadicarbaborane [μ-6,9-{$AlEt(OEt_2)$}-*nido*-6,9-$C_2B_8H_{10}$], for which the reported ^{11}B chemical shift data are unassigned, but which can be taken to represent a purely μ-6,9-bridged ten-vertex *nido* structure, with no additional complications from additional metal valence-electron participation as entertained above (Section *3*) for the platinum species **1** – **3**.

In accord with this last idea, it is apparent (Fig. 6, lower traces) that the ^{11}B cluster chemical shifts, and therefore, presumably, the cluster electronic structure, of the {$C_2B_8H_{10}$} fragment in the {$SnMe_2$} compound both clearly parallel those of the unmetallated [*nido*-6,9-$C_2B_8H_{10}]^{2-}$ substrate, thus supporting the conclusions that the {$SnMe_2$} residue reasonably constitutes an innocent μ-6,9-bridging group, and that the basic [*nido*-6,9-$C_2B_8H_{10}]^{2-}$ cluster electronic structure is thereby little perturbed[26]. The metal centre thereby has a two-orbital bonding interaction with the {$C_2B_8H_{10}$} cluster. By contrast (Fig. 6, upper traces) there is an equally clear parallel between the cluster

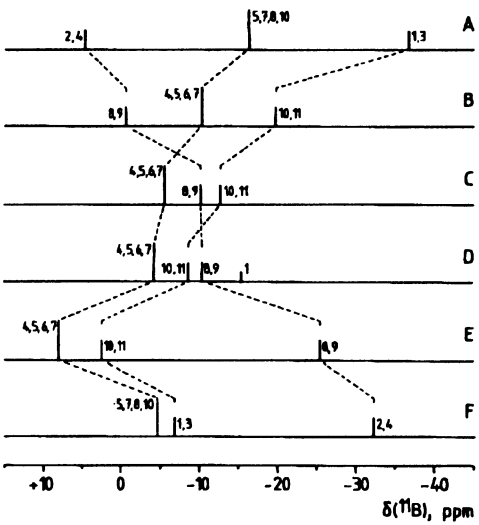

FIG. 6

Stick diagrams of the relative intensities and chemical shifts in the ^{11}B NMR spectra of (A) [*arachno*-6,9-$C_2B_8H_{14}$], (B) [1,1-$PMe_2Ph)_2$-1,1,3-$PtC_2B_8H_{10}$] (compound **1**), (C) [1,1-$(PPh_3)_2$-1,2,3-$PtC_2B_8H_{10}$] (compound **4**), (D) [*closo*-2,3-$C_2B_9H_{11}$], (E) [1,1-Me_2-1,2,3-$SnC_2B_8H_{10}$], and (F) the [*nido*-6,9-$C_2B_8H_{10}]^{2-}$ anion

TABLE VIII

Boron-11 and proton NMR measurements on the $Na_2[6\text{-R-}nido\text{-}6,9\text{-}C_2B_8H_9]$ (where R = H, Me, and Ph) compounds in CD_3CN solution at 294 – 297 K

Assignment[a]	$Na_2[6\text{-Me-}6,9\text{-}C_2B_8H_9]$				$Na_2[6,9\text{-}C_2B_8H_{10}]$			$Na_2[6\text{-Ph-}6,9\text{-}C_2B_8H_9]$		
	$\delta(^{11}B)$	$\delta(^1H)^b$	$^1J(^{11}B\text{-}^1H)$	Observed $[^1H\text{-}^1H]$-COSY correlations[c]	$\delta(^{11}B)$	$\delta(^1H)^b$	$^1J(^{11}B\text{-}^1H)$	$\delta(^{11}B)$	$\delta(^1H)^b$	$^1J(^{11}B\text{-}^1H)$
1,3	−1.9	+1.85	–[d]	2 m; 4 s	−6.9	+1.88	129	−6.7	+2.01	–[d]
2	−21.2	+0.15	137	1,3 m; 5,7 m				−26.2	+0.39	141
					−32.2	−0.07	138			
4	−29.0	+0.26	138	1,3 s; 8,10 s; 9 s				−31.5	−0.21	139
5,7	+1.9	+1.95	–[d]	2 m				−4.1	+2.36	–[d]
					−4.7	+2.09	122			
8,10	+0.4	+2.00	–[d]	4 s; 9 s				−4.7	+2.16	–[d]
6	[CMe]	+1.87	–	–				[CPh]	+7.48 – +6.87[e]	–
					[CH]	+4.26	–			
9	[CH]	+4.14	–	4 s; 8,10 s				[CH]	+4.47	

[a] Assignments based on relative intensities and observed $[^1H\text{-}^1H]$-COSY correlations for the 6-Me compound. [b] Related to directly bound boron positions by $^1H\text{-}\{^{11}B(\text{selective})\}$ experiments. [c] Observed under conditions of $\{^{11}B(\text{broad band noise})\}$ decoupling. [d] Value uncertain due to peak overlap. [e] Range of Ph signals (relative intensity 5H).

^{11}B shielding patterns of unmetallated ten-vertex {*arachno*-6,9-$C_2B_8H_{14}$] and the unsubstituted {$Pt(PMe_2Ph)_2$} eleven-vertex platinadicarbaborane compound **1**, demonstrating that the perturbation of the electronic structure of the initially *nido* [6,9-$C_2B_8H_{10}]^{2-}$ fragment towards *arachno* on platinum complexation to form compounds **1** – **3** is fundamental. This supports the supposition (Section *3* above) that there is considerable additional platinum valence-electron participation, over and above that which would be required for a simple platinum(II) bridge between the 6,9-positions in [*nido*-6,9-$C_2B_8H_{10}]^{2-}$ to give a product electronically analogous to [μ-6,9-($SnMe_2$)-*nido*-6,9-$C_2B_8H_{10}$] or [μ-6,9-{Al(OEt)Et}-*nido*-6,9-$C_2B_8H_{10}$]. The NMR similarities between **1** and [$C_2B_8H_{14}$] are in fact sufficiently close to suggest that the platinum compound be formally regarded as a platinum(IV) complex of the *arachno* tetradentate ligand {$C_2B_8H_{10}$}$^{4-}$ that would be formed by the notional deprotonation at the two bridging and the two *endo*-terminal sites in [$C_2B_8H_{14}$]. In this interpretation the four platinum-to-cluster two-electron bonding vectors would be approximately directed tangentially towards bonds with each of C(2) and C(3), and towards each of the mid-points of B(4)B(7) and B(5)B(6), with the two other positions in the octahedral eighteen-electron d^6 platinum(IV) coordination sphere occupied by the two phosphine ligands (structure *X*): the four bonds to bridging and *endo*-terminal hydrogen atoms in [$C_2B_8H_{14}$] are thus simply replaced by bonds to platinum, and the metal centre thereby has a four-orbital bonding interaction with the {$C_2B_8H_{10}$} cluster.

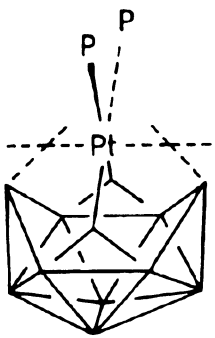

X

The shielding pattern of the {$Pt(PPh_3)_2$} and {$Pt(SEt_2)_2$} compounds **4** and **5** is clearly intermediate. There is characteristically an effective inversion of the assigned ^{11}B shielding pattern upon a ten-vertex *nido* → *arachno* intercomparison[23,27], and the patterns for compounds **4** and **5** lie close to the inversion point. The patterns are in fact remarkably close to that of the ostensibly classical *closo* species [2,3-$C_2B_9H_{11}$] (also included in Fig. 6), for which in the first instance a conventional three-orbital two-electron {BH(1)} cluster contribution may reasonably be invoked. Consequently a related

three-orbital two-electron platinum bonding interaction with the $\{C_2B_8H_{10}\}$ cluster can in turn be reasonably invoked for compounds **4** and **5**. This presumably arises from two strong bonds principally associated with C(2) and C(3), together with donor action of the B(4)B(7)/B(5)B(6) region into the vacant platinum(II) valence orbital. Although the longer platinum-to-boron distances discussed for compound **4** in Section *3* above suggest that this boron-to-metal interaction may not necessarily be particularly strong, it may be noted that BH(1) may be only weakly bonded to B(4)B(7)/B(5)B(6) in [2,3-$C_2B_9H_{11}$] itself. It is in this context noteworthy that in the structurally investigated C-methylated analogue [2,3-Me_2-*closo*-2,3-$C_2B_9H_9$] in the interboron distances from B(1) are long at 205 pm (ref.[28]), and the high fluxionality[29,30] of the isoelectronic congeners $[2\text{-}CB_{10}H_{11}]^-$ and $[B_{11}H_{11}]^{2-}$ also is thought to arise from the discomfort of BH(1) in this high-connectivity position[21].

Incidentally, it is convenient to note at this point the similarly intermediate NMR behaviour of the postulated[26] eleven-vertex "naked tin" stannadicarbaborane [1,2,3-$SnC_2B_8H_{10}$] (numbering as in structure *III*) that has seven- and twelve-vertex congeners in $[SnC_2B_4H_6]$ (ref.[31]) and $[SnC_2B_9H_{11}]$ (ref.[32]). These data also suggest accord with the conventional closed eleven-vertex $[C_2B_9H_{11}]$-type of electronic structure, consistent with the cluster-bonding principles for an unsubstituted tin atom discussed some time[33] ago for twelve-vertex [3,1,2-SnC_2B_9].

Another factor of principal interest in the NMR behaviour is that the C-methyl and C-phenyl compounds **2** and **3** were found to be fluxional in solution. Because of their asymmetry, each exhibits two P-methyl ^1H resonance positions at lower temperatures. Upon heating, each of these pairs coalesces to give one resonance position, but with

TABLE IX
Boron-11 and proton NMR measurements for [*closo*-2,3-$C_2B_9H_{11}$] in $CDCl_3$ solution at 294 – 297 K

Assignment	$\delta(^{11}B)$	$[^{11}B\text{-}^{11}B]$-COSY[a,b]	$^1J(^{11}B\text{-}^1H)$[c]	$\delta(^1H)$[c]	$[^1H\text{-}^1H]$-COSY[b,d]
1	−15.2	–	174	+1.19	2,3 s; 8,9 w[e]
2,3	[CH]	–	–	+5.94	1 s; 4,5,6,7 s; 8,9 mw; 10,11 vw[e]
4,5,6,7	−4.0	8,9 s; 10,11 w	170	+2.78	2,3 s; 8,9 m; 10,11 m
8,9	−10.3	4,5,6,7 s; 10,11 s	146	+2.08	1 w[e]; 2,3 m; 10,11 vs
10,11	−8.5	4,5,6,7 w; 8,9 s	168	+2.39	2,3 vw[e]; 4,5,6,7 m; 8,9 vs

[a] Observed under conditions of $\{^1H(\text{broad band noise})\}$ decoupling. [b] v very. [c] Related to directly bound boron positions by $^1H\text{-}\{^{11}B(\text{selective})\}$ experiments. [d] Observed under conditions of $\{^{11}B(\text{broad band noise})\}$ decoupling. [e] Interesting incidences of $^4J(^1H\text{-}^1H)$ coupling; all other correlations arise from ^3J cluster connectivity pathways.

TABLE X

NMR parameters for the eleven-vertex 1-stanna-2,3-dicarbaundecaboranes in CD_2Cl_2 solution at 294 – 297 K[a]

Assignment	$[Me_2SnC_2B_8H_{10}]$[b]		$[Ph_2SnC_2B_8H_{10}]$		$[Me_2SnC_2B_8H_9\text{-}2\text{-}Me]$[c]		$[SnC_2B_8H_{10}]$[d]	
	$\delta(^{11}B)$	$\delta(^1H)$	$\delta(^{11}B)$	$\delta(^1H)$	$\delta(^{11}B)$	$\delta(^1H)$	$\delta(^{11}B)$	$\delta(^1H)$
4,5,6,7	+8.1	+3.30	+7.5	+3.59	+8.4 +7.6	+3.19 +3.25	~ +0.2	+2.48
10,11	+2.5	+2.89	+4.1	+3.06	+1.6	+2.84	-6.1	+1.96
8,9	-25.5	+1.59	-25.8	+1.76	-19.7 -29.0	+1.63 +1.36	~ +0.5	+3.83
2,3	–	+4.61	–	+4.81	–	+4.41[e]	–	+6.30

[a] Data from ref.[26]; $\delta(^{11}B)$ and $\delta(^1H)$ both in ppm. [b] $\delta(^1H)(SnMe_2) = +0.92$, $^2J(^{119}Sn\text{-}^1H) = 65.7$ Hz. [c] $\delta(^1H)(SnMe_2) = 0.90$, $^2J(^{119}Sn\text{-}^1H) = 64.5$ Hz; $\delta(^1H)(CMe)(2) = 2.21$, $^3J(^{119}Sn\text{-}^1H) = 14.5$ Hz. [d] The 2-methyl derivative of this compound has $\delta(^1H)(3) = +6.65$, $\delta(^1H)(CMe)(2) = +2.68$, $^3J(^{119}Sn\text{-}^1H) = 26$ Hz. [e] Refers to 3-position.

retention of ^{195}P satellites, consistent with non-dissociative interchange of the two PMe_2Ph groups[34]. The observed solid-state configurations for compounds **1**, **2**, and **4** (Fig. 3) thence suggest that this arises from a geometrically straightforward rotational process. The rotation would be approximately about the axis through Pt(1) and the mid-point of the B(10)–B(11) linkage (structures *V*,*VI*, and *VII*), with no need to invoke additional gross cluster reconfiguration (other than the fluxing discussed above in Section *2*) such as the pentagonal face rotational process as postulated to account for observations[20] on the asymmetric analogue [10,10-$(PMe_3)_2$-*nido*-10,7,9-$PtC_2B_8H_{10}$] (Fig. 4). The derived activation parameters $\Delta G^{\neq}$ were 62.6 kJ mol^{-1} and 82.8 kJ mol^{-1} for the C-methyl and C-phenyl substituted compounds **2** and **3**, respectively, the higher figure for **3** reflecting the greater steric barrier to rotation caused by the larger C-phenyl versus C-methyl substituent at C(2) adjacent to the platinum atom. The observed comparative solid-state configurations of the compounds **2** and **3** (Fig. 3) suggest that the unsubstituted $\{Pt(PMe_2Ph)_2\}$ species **1** will also be fluxional, but its symmetry precluded its investigation by our method. Without C-substituent steric hindrance, in activation energy is probably much lower than for compounds **2** and **3**, probably in the region 30 – 40 kJ mol^{-1}. The unsubstituted $\{Pt(PPh_3)_2\}$ and $\{Pt(SEt_2)_2\}$ species **4** and **5** could also in principle be fluxional, but we have no experimental evidence. The non-twisted solid-state configuration of **4**, with the phosphorus atoms eclipsing CH(2) and CH(3) (Fig. 3, left and structure *V*) may, however, suggest quite a high rotational energy barrier or even effective non-fluxionality for this compound.

5. *Conclusions and Additional Structural Considerations*

The balance of the structural and NMR evidence (Section *2* and *3*), together with the electron-counting considerations (Section *4*), now suggest to us that the less compact cluster structure exhibited by the $\{Pt(PPh_3)_2\}$ compound **1** is now probably not best interpreted[4,5,7] in terms of square-planar platinum(II) and a simple bridged *nido* structure such as in main-group species such as $[Me_2SnC_2B_8H_{10}]$ and $\{Et(OEt)AlC_2B_8H_{10}\}$. Rather, it has much greater parallels with the classical[15] [*closo*-$B_{11}H_{11}]^{2-}$ type of structure, as exhibited by $[C_2B_9H_{11}]$ and $[Me_2C_2B_9H_9]$. It thereby has a basic three-orbital metal-to-cluster interaction, thus approximating closely to a conventional eleven-vertex Williams–Wade[1,15] species. The more compact ground-state cluster structure of the $\{Pt(PMe_2Ph)_2\}$ compounds **2** and **3**, by contrast, seems on present evidence to arise from an even greater metal-to-cluster interaction that involves a four-orbital bonding scheme. This type of interaction is not generally available for atoms of main-group elements in the 1-position of the eleven-vertex closed C_{2v} cluster, and the cluster type is therefore outside the scope of the straightforward[1,15] Wade–Williams cluster-geometry and electron-counting formalism.

These two cluster types constitute two points on a C_{2v} structural continuum, mentioned in the introduction to this paper, that proceeds from an *arachno*-type skeleton, as

in the $[\mu\text{-}6,9\text{-}(PPh_2)\text{-}arachno\text{-}B_{10}H_{12}]^-$ anion[2,3], to an *isocloso* skeleton, as in species such as $[\eta^5\text{-}C_5Me_5)IrB_{10}H_{10}]$ (ref.[35]). Across this series the unique heteroatom in the 1-position is held increasingly closely into the cluster (due allowance being made in this comparison for differences in atomic size among the elements constituting the compounds compared). There is some merit in briefly discussing members of this series in common context. So far there are five basic electronic types in the sequence:

1) In compounds of the first category, typified by the $[(PPh_2)_2B_{10}H_{12}]^-$ anion, there is no doubt of *arachno* character both in terms of NMR (ref.[3]) and structural[4] criteria. In this molecule the heteroatom in the 1-position has a basic two-orbital interaction with the cluster (structure *XI*).

2) The second set comprises species such as $\{Et(OEt)AlC_2B_8H_{10}]$ and $[Me_2SnC_2B_8H_{10}]$ that are reasonably described as bridged *nido* species both on structural grounds[10] and in terms of the NMR criteria discussed above (Section *4*). Again the unique heteroatom in the 1-position has a basic two-orbital interaction with the cluster (structure *XII*).

3) The next most compact species are the classic true *closo* species exemplified structurally by compounds such as $[2,3\text{-}Me_2\text{-}closo\text{-}2,3\text{-}C_2B_9H_9]$ (ref.[28]) and (presumably) $[closo\text{-}B_{11}H_{11}]^{2-}$ itself. In the present work this third structural type seems to be closely matched by $[(PPh_3)_2PtC_2B_8H_{10}]$ (compound **4**). The "naked tin" compound[26] $[SnC_2B_8H_{10}]$ is probably also in this category. This *closo* type is conventionally held to have a basic three-orbital involvement of the 1-position with the rest of the cluster, and the experimental evidence in this paper is not inconsistent with this in the case of compound **4** and its $\{Pt(SEt_2)_2\}$ analogue **5**. For this third category in the sequence, the Williams–Wade formalism[1,15] would also dictate that *closo*-1-metalladicarbaundecaboranes such as $[2\text{-}Me\text{-}1\text{-}(\eta^5\text{-}C_5Me_5)\text{-}closo\text{-}1,2,3\text{-}RhC_2B_8H_9]$ (ref.[7]) are true *closo*, and thus take a logical place here on the continuum, with a formal complete three-orbital involvement of the metal in the eleven-vertex *closo* cluster structure. However, it is of interest that both these[21] and also[10,19,36] the $[(PR_3)_2PtC_2B_8H_{10}]$ species discussed here will develop open faces and *nido*-type geometry if there is asymmetric heteroatom arrangement in the cluster (this is discussed briefly below).

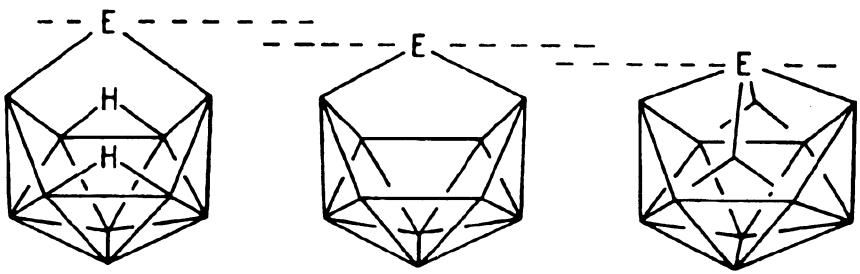

XI *XII* *XIII*

4) The fourth type on the sequence is exemplified, so far uniquely, by the ground-state configurations of the $\{Pt(PMe_2Ph)_2\}$ species **1** – **3** described in this present work. These clusters are more compact than those in the third category. Although of *closo* C_{2v} eleven-vertex geometry, they nevertheless have a *nido* count for the electrons that are involved in the cluster bonding proper. The extra hyper-Wadian electron pair is involved in an additional metal-to-borane bonding orbital, with the metal atom in the 1-position thereby achieving a four-orbital bonding involvement and a concomitant closer binding with the rest of the cluster (structure *XIII*).

5) Compounds in the fifth and final category consist of the so-called "*isocloso*" eleven-vertex species such as [1-(η^5-C_5Me_5)-*isocloso*-1-$IrB_{10}H_{10}$] (ref.[35]) and [2,3-$(OMe)_2$-1,1-$(PMe_2Ph)_2$-μ-1,2-H-*isocloso*-1-$RhB_{10}H_8$] (ref.[37]). These also have a compact metal-to-borane binding that is believed to entail a hyper-Wadian four-orbital cluster bonding involvement of the metal atom in the 1-position (again as in structure *XIII*). The fourth orbital is invoked to generate a *closo* electron-count[38], and seems compatible with structural evidence where suitable compounds have been examined[37].

Both these last two categories are of interest because the four-orbital metal-to-cluster interaction is not covered by the Williams–Wade cluster formalism, and it would be helpful to see rigorous molecular orbital treatments in this area.

An additional important general structural point associated with the foregoing concerns the structural distortions which appear to be induced by any asymmetric arrangement of cluster constituents in the "true" *closo* eleven-vertex clusters in category three. The origin of this arises because the eleven-vertex Wadian *closo* cluster-electron count seems to be basically uncomfortable in the C_{2v} eleven-vertex *closo* cluster shape, indicating that the grip of the Williams–Wade formalism may be quite tenuous in this particular area. The basic $[B_{11}H_{11}]^{2-}$ dianion itself[30], as well as closely related species such as the $[CB_{10}H_{11}]^-$, $[B_{11}H_{10}(SMe_2)]^-$, and $[B_{11}H_9(Se_3)]^{2-}$ anions[29,39,40], are fluxional in solution, probably via open-faced structures which must have similar energies to the classical *closo* one[21,41]. Also, the two formally *closo* species [1-(η^5-C_5H_5)-*closo*-1,2-$FeCB_9H_{10}]^-$ and [1-(η^6-MeC_6H_4iPr)-*closo*-1,2-$RuNB_9H_{10}$], where the sites of a symmetry are localized on the cluster mirror planes, exhibit marked lengthening of the metal-cluster linkages around the heteroatom (structure *XIV*)[42,43]. When the site of the asymmetry

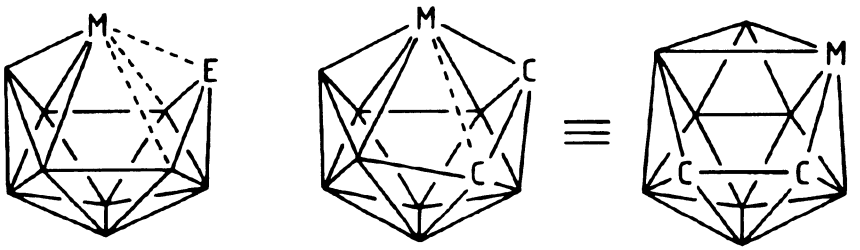

XIV *XVa* *XVb*

in metallaheteroboranes like these is off-plane, as in the (formally) *closo* {1,2,4-$M_2C_2B_8$} cluster compounds such as [1,1,1-$(PPh_3)_2$H-1,2,4-$IrC_2B_8H_{10}$] (ref.[21]) then a marked distortion to an open "*isonido*" cluster with a four-membered open face is favoured (structures *XVa* and *XVb*); this *isonido* cluster type *XV* is a good approximation to the structures of intermediates reasonably postulated[21,29] for fluxionality of the $[B_{11}H_{11}]^{2-}$ anion. Any tendency to metal square-planar character in combination with this asymmetry can induce further opening to classical *nido* eleven-vertex geometry, as in [10,10-$(PMe_3)_2$-*nido*-10,7,9-$PtC_2B_8H_{10}$] (Fig. 4 and structure *XVI*)[19,20], and this tendency is enhanced when the open-face can have bridging hydrogen atoms, as in [8,8-$(PMe_2Ph)_2$-*nido*-8,7-$PtCB_9H_{11}$] (ref.[44]) and [8,8-$(PPh_3)_2$-*nido*-8,7-$RhSB_9H_{11}$] (ref.[45]) (structure *XVII*), and as in [9,9-$(PPh_3)_2$-*nido*-9,8,7-$RhC_2B_8H_{12}$] (structure *XVIII*)[46]. These last three compounds are of particular interest because their structures are energetically very close to more closed isomeric structures.

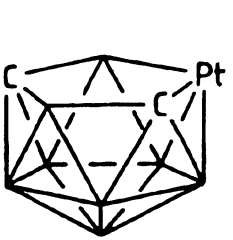

XVI

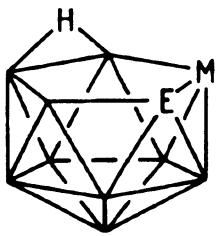

XVII

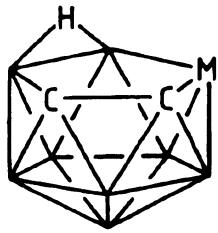

XVIII

Thus the {RhC_2B_8} species exists in equilibrium[47] with its "*closo*" isomer [1,1,1-$(PPh_3)_2$H-1,2,4-$RhC_2B_8H_{10}$] (probably of "*isonido*" geometry *XV*), and other two species are fluxional between enantiomers in a manner that implies closed isomeric intermediates of approximate structure *XIV* (refs[44,45]).

EXPERIMENTAL

Preparation of [2-X-1,1-$(PMe_2Ph)_2$-1,2,3-$PtC_2B_8H_9$] where X = H (Compound **1**), Me (Compound **2**), and Ph (Compound **3**)

The procedure is described in detail for compound **1**. $Na_2[6,9\text{-}C_2B_8H_{10}]$ (50 mg, 290 μmol, prepared as in ref.[48]) was added in one portion to a solution of $[PtCl_2(PMe_2Ph)_2]$ (119 mg, 219 μmol) in CH_2Cl_2 (10 cm^3; degassed and freshly distilled from P_4O_{10}). A yellow colour developed almost immediately. The mixture was stirred at ambient temperature under N_2 for 20 h, then filtered in air to remove NaCl and excess $Na_2[6,9\text{-}C_2B_8H_{10}]$. The yellow filtrate was evaporated in vacuo with silica gel (column grade, ca 3 g) and the resultant solids placed on the top of a chromatographic column packed with silica gel (2.5 × 15 cm). Chromatography was carried out with 30 : 70 CH_2Cl_2–C_6H_6 and monitored by analytical TLC. An initial colourless component was [*arachno*-4,6-$C_2B_7H_{13}$] (discarded). The principal product was a yellow fraction. This was evaporated to dryness, the resulting

yellow solid dissolved in CH_2Cl_2 (ca 2 cm^3) and purified by preparative TLC on silica, using 40 : 60 C_6H_{12}–CH_2Cl_2 as liquid phase. The main yellow band (R_F 0.44) was removed and extracted with CH_2Cl_2 (ca 5 cm^3). The extract was reduced in volume in vacuo to ca 3 cm^3, and hexane (ca 4 cm^3) was carefully overlayered. After three days the resulting large orange-yellow crystals were filtered off, dried in vacuo, and identified as [1,1-$(PMe_2Ph)_2$-1,2,3-$PtC_2B_8H_{10}$] (compound **1**) (67 mg, 52%). A second crop (8 mg, 6%, total yield 58% based on [$PtCl_2(PMe_2Ph)_2$]) was obtained by a similar procedure from the solid residues remaining after evaporation of the mother liquors. Similar procedures using Na_2[6-Me-6,9-$C_2B_8H_9$] and Na_2[6-Ph-6,9-$C_2B_8H_9$] (prepared in a similar way[48] to Na_2[6,9-$C_2B_8H_{10}$] from the corresponding C-methyl and C-phenyl starting materials) resulted in the formation of [2-Me-1,1-$(PMe_2Ph)_2$-1,2,3-$PtC_2B_8H_9$] (compound **2**) and [2-Ph-1,1-$(PMe_2Ph)_2$-1,2,3-$PtC_2B_8H_9$] (compound **3**) respectively as orange-yellow crystalline compounds. Compound **2** (TLC R_F 0.50; silica, 40 : 60 C_6H_{12}–CH_2Cl_2 as liquid phase) was obtained in a yield of 59% and compound **3** (TLC R_F 0.15; silica, 60 : 40 C_6H_{12}–CH_2Cl_2 as liquid phase) in a yield of 88% (reaction scales 221 μmol and 66 μmol in [$PtCl_2(PMe_2Ph)_2$], respectively). Incidental to this work we recorded and assigned the ^{1}H NMR chemical shifts of the [*nido*-6,9-$C_2B_8H_{10}$]$^{2-}$ and [6-Me-*nido*-6,9-$C_2B_8H_9$]$^{2-}$ anions, which are presented in Table VIII, and of [*closo*-2,3-$C_2B_9H_{11}$], presented in Table IX. Crystals of compounds **1** and **2** suitable for single-crystal X-ray diffraction analysis were obtained from dichloromethane–hexane.

TABLE XI

Fractional atomic coordinates (. 10^4) and equivalent isotropic thermal parameters (in pm^2) for [1,1-$(PMe_2Ph)_2$-1,2,3-$PtC_2B_8H_{10}$] (**1**) with e.s.d.'s in parentheses

Atom	*x*	*y*	*z*	U_{eq}[a]
Pt(1)	7500[b]	-1111.9(3)	0[b]	27.5(2)
P(1)	6711(1)	444(2)	391(2)	41.0(7)
C(11)	7122(6)	1855(11)	1173(9)	69(4)
C(12)	6024(6)	-128(11)	1121(9)	69(4)
C(131)	6131(5)	1172(7)	-742(9)	46(3)
C(132)	6065(5)	540(9)	-1691(8)	59(3)
C(133)	5611(9)	1076(11)	-2581(14)	93(6)
C(134)	5199(6)	2214(14)	-2461(13)	89(5)
C(135)	5242(7)	2792(13)	-1521(16)	97(7)
C(136)	5720(6)	2312(11)	-650(10)	78(5)
C(2)	7799(5)	-2501(9)	-1075(7)	50(3)
B(4)	6954(6)	-3016(11)	-1190(8)	57(4)
B(5)	8358(7)	-2923(12)	-87(9)	58(4)
B(8)	7786(11)	-4059(15)	-953(13)	74(6)
B(10)	7016(9)	-4416(15)	-380(11)	78(6)

[a] U_{eq} is defined as one third of the trace of the orthogonalized $\boldsymbol{U}_{ij}$ matrix. [b] Coordinate fixed on special position.

TABLE XII

Fractional atomic non-hydrogen coordinates (. 10^4) and equivalent isotropic thermal parameters (in pm^2) together with cluster hydrogen coordinates (. 10^3) and their isotropic thermal parameters (in pm^2 . 10^{-1}) for [1,1-(PMe_2Ph)$_2$-1,2,3-$PtC_2B_8H_9$-2-Me] (**2**) with e.s.d.'s in parenthesis

Atom	*x*	*y*	*z*	U_{eq}[a]
Pt(1)	6925.0(1)	3309.4(1)	3455.6(1)	32.2(1)
P(1)	4711(1)	3245(1)	3744(1)	36.2(3)
P(2)	8153(1)	2633(1)	4560(1)	46.5(3)
C(11)	3181(4)	3550(3)	2946(2)	51.4(14)
C(12)	4427(5)	3960(3)	4495(2)	51(2)
C(131)	4158(3)	2171(1)	3973(2)	41.2(13)
C(132)	3549(3)	2005(1)	4586(2)	54(2)
C(133)	3112(3)	1169(1)	4712(2)	77(2)
C(134)	3285(3)	498(1)	4225(2)	81(3)
C(135)	3894(3)	664(1)	3613(2)	76(3)
C(136)	4331(3)	1501(1)	3487(2)	57(2)
C(21)	8036(8)	1455(3)	4547(4)	86(3)
C(22)	10116(5)	2811(5)	4818(3)	74(2)
C(231)	7663(3)	2966(2)	5430(1)	44.9(13)
C(232)	6752(3)	2469(2)	5757(1)	60(2)
C(233)	6323(3)	2778(2)	6393(1)	74(2)
C(234)	6807(3)	3584(2)	6701(1)	78(2)
C(235)	7718(3)	4081(2)	6374(1)	70(2)
C(236)	8147(3)	3772(2)	5739(1)	54(2)
C(2)	7532(5)	4638(3)	3266(2)	49.8(14)
C(21)	7507(9)	5372(3)	3822(4)	74(3)
C(3)	7115(5)	2556(3)	2468(2)	45(2)
B(4)	6255(6)	4438(3)	2533(3)	49(2)
B(5)	8920(6)	4106(3)	3230(3)	53(2)
B(6)	8694(5)	2921(3)	2790(3)	45(2)
B(7)	6011(6)	3266(3)	2086(3)	49(2)
B(8)	8006(6)	4795(3)	2449(3)	56(2)
B(9)	7685(6)	3061(3)	1801(3)	48(2)
B(10)	6983(6)	4116(3)	1751(3)	53(2)
B(11)	8902(6)	3868(3)	2246(3)	50(2)

TABLE XII
(*Continued*)

Atom	*x*	*y*	*z*	U_{eq} [a]
H(21a)	817(6)	538(4)	424(3)	10(2)
H(21b)	815(8)	594(5)	367(4)	11(3)
H(21c)	647(7)	552(4)	382(3)	12(2)
H(3)	699(5)	208(3)	244(3)	6(2)
H(4)	522(4)	480(3)	239(2)	4.5(11)
H(5)	999(5)	424(3)	365(3)	7.3(14)
H(6)	966(5)	256(3)	301(3)	8(2)
H(7)	498(5)	309(3)	172(2)	4.9(11)
H(8)	845(4)	541(3)	244(3)	5.9(12)
H(9)	773(5)	270(3)	123(3)	6.3(13)
H(10)	655(5)	442(3)	114(3)	7.0(13)
H(11)	980(4)	397(3)	202(2)	4.9(11)

[a] U_{eq} is defined as one third of the trace of the orthogonalized $\boldsymbol{U}_{ij}$ matrix.

Nuclear Magnetic Resonance Spectroscopy

NMR spectroscopy was carried out at 2.35 (100 MHz ^{1}H) or 9.4 Tesla (400 MHz ^{1}H) on commercially acquired instrumentation, with the techniques of ^{1}H-{^{11}B(selective)} (ref.[22]) and [^{1}H-^{1}H]-COSY-{^{11}B} (ref.[49]) spectroscopy, and also the general techniques, being essentially as described and exemplified in more detail in other recent papers that deal with NMR work from our laboratories[34,50 - 52]. Chemical shifts δ are given in ppm to high frequency (low field) of Ξ = 100 ($SiMe_4$) for ^{1}H (quoted ±0.05 ppm) Ξ = 40.480 730 (nominally 85% H_3PO_4) for ^{31}P (quoted ±0.5 ppm), Ξ = 32.083 971 (nominally F_3BOEt_2 in $CDCl_3$) for ^{11}B (quoted ±0.5 ppm), and Ξ = 21.4 MHz (the Goodfellow frequency)[53] for ^{195}Pt, Ξ being defined as in ref.[54]. Spectra were calibrated for δ by using solvent deuteron or residual proton resonances as internal secondary standards. Given values of $^1J(^{11}B\text{-}^1H)$/Hz were measured from the resolution-enhanced ^{11}B traces, digital resolution 8 Hz.

Single-Crystal X-Ray Diffraction Analysis

All crystallographic measurements were made on a Nicolet P3/F diffractometer operating in the ω scan mode using graphite-monochromated MoK_αX-radiation[55]. The structure of each of compounds **1** and **2** was determined via standard heavy-atom methods and refined by full-matrix least squares[56]. All non-hydrogen atoms for each complex were refined with anisotropic thermal parameters. The phenyl and methyl hydrogen atoms of compound **2** were included in calculated positions and assigned to an overall isotropic thermal parameter, and the cluster hydrogen atoms of this compound were located on a Fourier difference synthesis and refined with individual isotropic thermal parameters. Hydrogen atoms were not locatable for compound **1** but were apparent from NMR spectros-

copy (Section *4* above; Table VI). The weighting scheme $w = [\sigma^2(F_o) + 0.0004(F_o)^2]^{-1}$ was used for each compound. Final atomic coordinates are listed in Table XI for **1** and Table XII for **2**.

Crystal data for compound 1. $C_{18}H_{32}B_8P_2Pt$, M = 591.7, monoclinic, space group *I2/a* (= *C2/c*), a = 1 824.8(2), b = 1 016.8(2), c = 1 328.2(3) pm, β = 101.48(2)°, V = 2.4150(8) nm^3, Z = 4, D_c = 1.63 Mg m^{-3}, μ = 57.00 cm^{-1}, $F(000)$ = 1 152, R (R_w) = 0.0442 (0.0474) for the refinement of 2 057 unique absorption-corrected[57] reflections with $I > 2.0\sigma(I)$ and 4.0 < 2θ < 50.0°.

Crystal data for compound 2. $C_{19}H_{34}B_8P_2Pt$, M = 606.0, monoclinic, space group $P2_1/n$, a = 947.6(1), b = 1 547.7(3), c = 1 804.0(3) pm, β = 104.78(1)°, V = 2.5581(8) nm^3, Z = 4, D_c = 1.57 Mg m^{-3}, μ = 53.82 cm^{-1}, $F(000)$ = 1 184, R (R_w) = 0.0216 (0.234) for the refinement of 2 057 unique absorption-corrected[57] reflections with $I > 2.0\sigma(I)$ and 4.0 < 2θ < 50.0°.

The authors wish to thank the SERC, the Royal Society, Borax Research Limited, and the Grant Agency of the Academy of Sciences of the Czech Republic (Grant No. 43204) for support, and Drs J. B. Farmer and T. S. Griffin for helpful cooperation.

REFERENCES

1. Wade K.: J. Chem. Soc., Chem. Commun. *1971*, 792; Wade K.: Adv. Inorg. Chem. Radiochem. *18*, 1 (1976).
2. Beckett M. A., Kennedy J. D.: J. Chem. Soc., Chem. Commun. *1983*, 575.
3. Thornton-Pett M., Beckett M. A., Kennedy J. D.: J. Chem. Soc., Dalton Trans. *1986*, 303.
4. Štíbr B., Janoušek Z., Baše K. Heřmánek S., Plešek J., Zakharova I. A.: Collect. Czech. Chem. Commun. *49*, 1891 (1984).
5. Kukina G. A., Porai-Koshits M. A., Sergienko V. C., Štrouf O., Baše K., Zakharova I. A., Štíbr B.: Izv. Akad. Nauk SSSR, Ser. Khim. *1980*, 1686.
6. Kukina G. A., Porai-Koshits M. A., Sergienko V. C.: Koord. Khim. *12*, 561 (1986).
7. Ditzel E. J., Fontaine X. L. R., Greenwood N. N., Kennedy J. D., Sisan Z., Štíbr B., Thornton-Pett M., : J. Chem. Soc., Chem. Commun. *1990*, 1741.
8. Fontaine X. L. R., Fowkes H., Greenwood N. N., Kennedy J. D., Thornton-Pett M.: J. Chem. Soc., Dalton Trans. *1987*, 2417.
9. Kennedy J. D., Štíbr B., Thornton-Pett M., Jelínek T.: Inorg. Chem. *30*, 4481 (1991); Nestor K., Zammitt G. S. A., Jelínek T., Thornton-Pett M., Kennedy J. D., Štíbr B.: J. Organomet. Chem. *477*, C1 (1992).
10. Schubert D. M., Knobler C. B., Rees W. S., Hawthorne M. F.: Organometallics *6*, 201 (1987).
11. Kennedy J. D.: Prog. Inorg. Chem. *34*, 211 (1988).
12. Grimes R. N. in: *Comprehensive Organometallic Chemistry* (G. Wilkinson, F. G. A. Stone and E. Abel, Eds), Part I., Chap. 5.5, p. 459. Pergamon Press, 1982.
13. Tippe A., Hamilton W. C.: Inorg. Chem. *8*, 464 (1969).
14. Kendall D. S., Lipscomb W. N.: Inorg. Chem. *12*, 546 (1973).
15. Williams R. E.: Inorg. Chem. *10*, 210 (1971). Williams R. E.: Adv. Inorg. Chem. Radiochem. *18*, 67 (1976).
16. Faridoon, Ni Dhubhghaill O., Spalding T. R., Ferguson G., Fontaine X. L. R., Kennedy J. D.: J. Chem. Soc., Dalton Trans. *1989*, 1657.
17. Kennedy J. D.: Main Group Met. Chem. *12*, 149 (1989).
18. McInnes Y. M., Thornton-Pett M.: *Proceedings of the Sixth International Meeting on Boron Chemistry, IMEBORON VI, Bechyně 1987*, abstr. No. 16.

19. Barker G. K., Green M., Spencer J. L., Stone F. G. A., Taylor B. F., Welch A. J.: J. Chem. Soc., Chem. Commun. *1974*, 804.
20. Green M., Spencer J. L., Stone F. G. A.: J. Chem. Soc., Dalton Trans. *1979*, 1680.
21. Nestor K., Fontaine X. L. R., Greenwood N. N., Kennedy J. D., Plešek J., Štíbr B., Thornton-Pett M.: Inorg. Chem. *28*, 2219 (1989).
22. Fontaine X. L. R., Kennedy J. D.: J. Chem. Soc., Dalton Trans. *1987*, 1573.
23. Bown M., Fontaine X. L. R., Kennedy J. D.: J. Chem. Soc., Dalton Trans. *1988*, 1467.
24. Fontaine X. L. R., Greenwood N. N., Kennedy J. D., MacKinnon P., Thornton-Pett M.: J. Chem. Soc., Dalton Trans. *1988*, 2809.
25. Nestor K., Jelínek T., Fontaine X. L. R., Kennedy J. D., Thornton-Pett M., Baše K., Štíbr B.: J. Chem. Soc., Dalton Trans. *1990*, 2887.
26. Štíbr B., Kennedy J. D.: *Ninth Meeting of the Silicon, Germanium, Tin and Lead Discussion Group (Royal Society of Chemistry), London 1989*, P4.; Nestor K., Štíbr B., Jelínek T., Kennedy J. D.: J. Chem. Soc., Dalton Trans. *1993*, 1661.
27. Beckett M. A., Kennedy J. D.: J. Chem. Soc., Chem. Commun. *1983*, 575.
28. Tsai C., Streib W. E.: J. Am. Chem. Soc. *88*, 4513 (1966).
29. Wiersema R. J., Hawthorne M. F.: Inorg. Chem. *12*, 785 (1973).
30. Tolpin E. I., Lipscomb W. N.: J. Am. Chem. Soc. *95*, 2384 (1973).
31. Wong K-S., Grimes R. N.: Inorg. Chem. *16*, 2053 (1977).
32. Rudolph R. W., Voorhees R. L., Cochoy R. E.: J. Am. Chem. Soc. *92*, 3351 (1970).
33. Rudolph R. W., Chowdhry V.: Inorg. Chem. *13*, 248 (1974).
34. Ferguson G., Kennedy J. D., Fontaine X. L. R., Faridoon, Spalding T. R.: J. Chem. Soc., Dalton Trans. *1988*, 2555.
35. Nestor K., Petříček V., Thornton-Pett M.: Unpublished results.
36. Jones J. H.: Unpublished results.
37. Fowkes H., Greenwood N. N., Kennedy J. D., Thornton-Pett M.: J. Chem. Soc., Dalton Trans. *1986*, 517.
38. Kennedy J. D.: Inorg. Chem. *25*, 111 (1986).
39. Wong E. H., Prasad L., Gabe E. J., Gatter M. G.: Inorg. Chem. *22*, 1143 (1983).
40. Friesen G. D., Little J. L., Huffmann J. C., Todd L. J.: Inorg. Chem. *18*, 755 (1979).
41. Leonowicz M. E., Scholer F. R.: Inorg. Chem. *19*, 122 (1980).
42. Baše K., Bown M., Štíbr B., Fontaine X. L. R., Greenwood N. N., Kennedy J. D., Thornton-Pett M.: J. Chem. Soc., Chem. Commun. *1988*, 1240.
43. Šubrtová V., Línek A., Hašek J.: Acta Crystallogr., B *34*, 2720 (1978).
44. Štíbr B., Jelínek T., Kennedy J. D., Fontaine X. L. R., Thornton-Pett M.: J. Chem. Soc., Dalton Trans., in press.
45. Ferguson G., Jennings M. C., Lough A. J., Coughlan S., Spalding T. R., Fontaine X. L. R., Kennedy J. D., Štíbr B.: J. Chem. Soc., Chem. Commun. *1990*, 891.
46. Lu P., Knobler C. B., Hawthorne M. F.: Acta Crystallogr., C *40*, 1704 (1984).
47. Jung C. W., Hawthorne M. F.: J. Am. Chem. Soc. *102*, 3024 (1980).
48. Štíbr B., Plešek J., Heřmánek S.: Collect. Czech. Chem. Commun. *38*, 338 (1973).
49. Fontaine X. L. R., Kennedy J. D.: J. Chem. Soc., Chem. Commun. *1986*, 779.
50. Faridoon, Ni Dhubhghaill O., Spalding T. R., Ferguson G., Fontaine X. L. R., Kennedy J. D.: J. Chem. Soc., Dalton Trans. *1989*, 1657.
51. Bown M., Plešek J., Baše K., Štíbr B., Fontaine X. L. R., Greenwood N. N., Kennedy J. D.: Magn. Reson. Chem. *27*, 947 (1989).
52. Fontaine X. L. R., Kennedy J. D., McGrath M., Spalding T. R.: Magn. Reson. Chem. *29*, 711 (1991).

53. Kidd R. G., Goodfellow R. J. in: *NMR and the Periodic Table* (R. K. Harris and B. E. Mann., Eds), Chap. 8, p. 250. Academic Press, 1978.
54. McFarlane W.: Proc. R. Soc. London, A *306*, 185 (1968).
55. Modinos A., Woodward P.: J. Chem. Soc., Dalton Trans. *1974*, 2065.
56. Sheldrick G. M.: *SHELX 76, Program System for X-Ray Structure Determination.* University of Cambridge, Cambridge 1976.
57. Walker N., Stuart D.: Acta Crystallogr., A *39*, 158 (1983).

Translated by the author (B. Š.).